International Journal of Greenhouse Gas Control 83 (2019) 166–175

Contents lists available at ScienceDirect

International Journal of Greenhouse Gas Control

journal homepage: www.elsevier.com/locate/ijggc

# Study of a full scale oxy-fuel cement rotary kiln

Mario Ditaranto*, Jørn Bakken

*SINTEF Energi AS, Postboks 4761 Torgarden, 7465, Trondheim, Norway*

ARTICLE INFO

*Keywords:*
Oxy-fuel combustion
Cement rotary kiln

ABSTRACT

Oxy-fuel combustion has been shown to be an attractive technology to be implemented in cement production with $CO_2$ capture from a process point of view. Due to the market situations and future perspectives it is necessary that the technology can be retrofitted into existing plants. As part of the H2020 EU project CEMCAP, the study presented here investigates the retrofitting of oxy-fuel combustion technology on a typical full-scale cement rotary kiln of 3000 ton/year clinker capacity. The flame generated by a commercial burner has been modelled by CFD with a seven steps combustion reaction model, the k-omega SST turbulence model, and the discrete ordinates radiation model with the Weighted Sum Grey Gas model. The burner is composed of an annular outlet where coal is fed and nozzles from which angled high velocity jets generate a swirling motion for flame stabilization and mixing purposes. As in all rotary cement kilns, a high temperature low velocity secondary oxidizer stream coming from the clinker cooler flows coaxially to the burner in the kiln for heat efficiency purposes. A flame developing in air has been used as a reference case and several oxy-fuel flames have been characterized and compared. The oxy-fuel inlet parameters that are varied in the study are the oxidizer composition and flow rates in both the primary and secondary streams. The work presented is part of an optimization procedure based on iterative interaction with the process modelling of the whole cement plant with full oxy-fuel capture (not presented in this article). With retrofit application in mind, the objective was to reproduce a heat radiation profile to the clinker equivalent to that obtained in the air reference case. The optimized oxy-fuel case is characterized by a primary burner oxidizer of lower flow rate, but with higher oxygen concentration of up to 52.1% to generate the necessary heat in the near burner region.

## 1. Introduction

Cement production is responsible for approximately 8% of the global $CO_2$ emissions (IPCC, 2006) and the use of the cement is expected to grow with industrialization and increased urbanisation in all parts of the world. While $CO_2$ emissions are generally related to the energy demand of an industrial process, 60% of emissions in cement production is a consequence of the transformation of limestone to lime (the calcination process), and 40% is due to combustion for providing necessary heat. Schneider et al. (2011) maps all the technical potential measures for $CO_2$ reduction in the cement production, and although energy efficiency and more extensive use of waste as raw materials can improve the $CO_2$ footprint in cement production, as was the case in Poland with a reduction of 28% through the 1998–2008 period (Deja et al., 2010), they will always have limited effect in that industrial sector. Carbon Capture and Storage (CCS) is the only technology that allows dramatic $CO_2$ emissions reduction according to Leeson et al. (2017) and Hills et al. (2016) who reviewed studies with claimed emissions captured ranging from 50% to 94% depending on the capture technology applied. According to the International Energy Agency (IEA) scenario (IEAGHG(TCP), 2018), by 2050 48% of the emission reduction in the cement sector should be contributed by the application of CCS to achieve the so-called 2 ° Scenario (2DS) target. Two capture schemes can be used for that purpose: post-combustion and oxy-fuel capture technologies with costs ranging from 17 to 164.6 $/t, as reviewed by Leeson et al. (2017). The oxy-fuel capture technology has been evaluated by an IEA study to be 41.2 $/t (IEAGHG(TCP), 2013). Gerbelova et al. (2017) investigated the total capital investment and the annual operation and maintenance costs of both post-combustion and oxy-fuel $CO_2$ capture systems and concluded that the latter may be a better choice in terms of costs. They recognized however that this technology implies higher technical uncertainties concerning integration with the cement plant. The oxy-fuel capture technology has raised particular focus when the European Cement Research Academy (ECRA) announced in 2018 that the technology will be implemented in two cement plants in Europe in the Colleferro (Italy) and Retznei (Austria) sites.

The oxy-fuel $CO_2$ capture technology is based on combustion of the

* Corresponding author.
*E-mail address:* mario.ditaranto@sintef.no (M. Ditaranto).

https://doi.org/10.1016/j.ijggc.2019.02.008
Received 17 August 2018; Received in revised form 22 January 2019; Accepted 12 February 2019

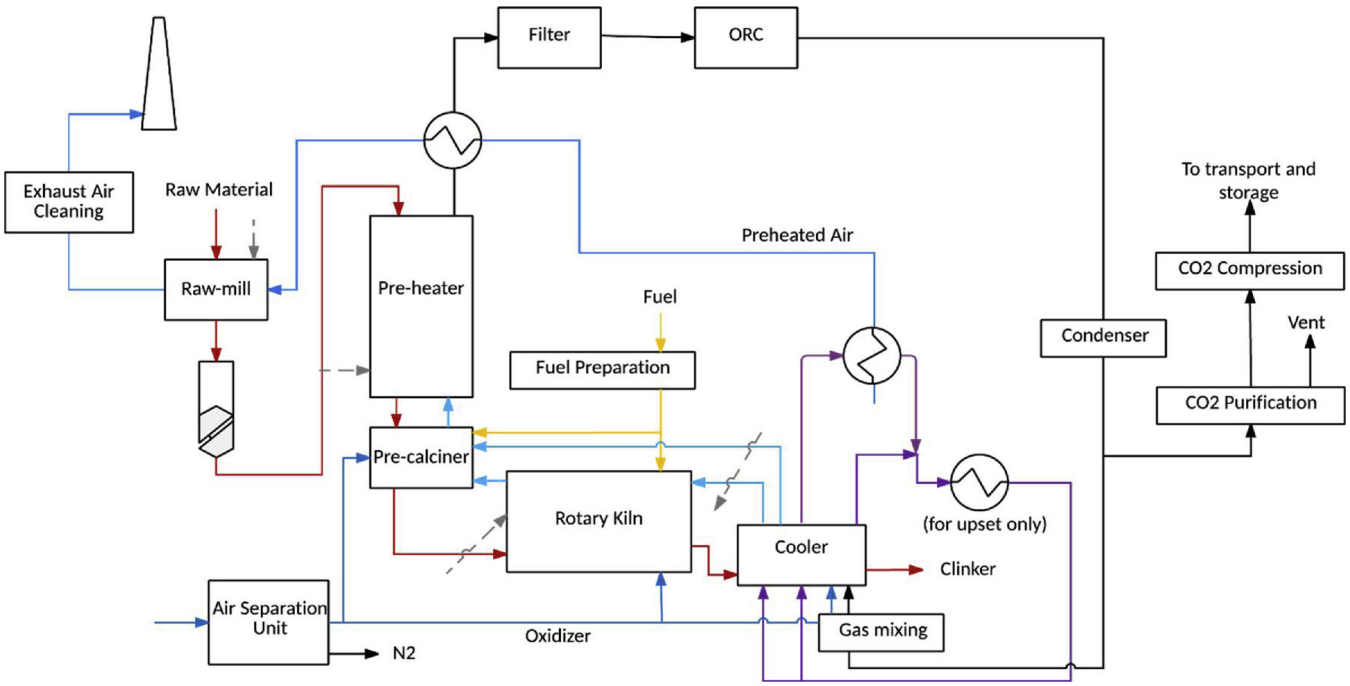


**Fig. 1.** Cement making plant in full oxy-fuel mode showing process components, gas and clinker streams in full lines and potential air leaks in dashed lines (from European Cement Research Academy).

fuel in an atmosphere of oxygen and recirculated flue gas (mainly $CO_2$) instead of air. The flue gases are then ideally composed of water vapour and $CO_2$ which are easily and cheaply separated by condensation, as compared to a conventional combustion with a post-treatment capture scheme, where $CO_2$ is only a minor component which requires energetically intensive chemical separation. The drawback and energy penalty in the oxy-fuel capture technology lies in the necessity to produce high purity oxygen (95%) in an Air Separation Unit (ASU) as shown in Fig. 1. The technology also implies adaption of the combustion equipment as moving the oxidizer composition from air has significant impact on the characteristics of the flame developed in the rotary kiln by affecting many combustion properties. Besides it is important that the heat transfer to the clinker remains the same to maintain product quality and process efficiency. ECRA investigated the impact of oxy-fuel combustion on clinker composition and properties and concluded that no major differences could be observed in its composition, structure, and properties (European Cement Research Academy, 2012). Zheng et al. (2016) showed also that good-quality cement can be successfully produced in an oxy-fuel atmosphere and it has similar phase and chemical compositions, and comparable compressive strength to commercially available cements.

Implementation of oxy-fuel technology to a cement plant also requires that the whole process is optimized for energy efficiency because the volumes and composition of gases flowing in the system are different from those of conventional plants. One main constraint is due to the fact that oxygen has a high energy cost of separation and must therefore be supplied in as near stoichiometric quantity as possible, making combustion completeness in the kiln more complicated. Finally, the prospect for new cement plants built in Europe being very poor, requires that CCS is implemented by retrofitting existing plants. Therefore major modifications of the rotary kiln are not envisageable and it must be possible to switch from air to oxy-fuel modes.

There has been significant research in oxy-fuel combustion of coal in the last decade motivated by the $CO_2$ capture from coal fired power generation and reviewed in Buhre et al. (2005) and Toftegaard et al. (2010). Even several large scale simulations have been performed in oxy-fuel mode, where for example Adamczyk et al. (2017) modelled a full scale 1000 $MW_{th}$ boiler by Computational Fluid Dynamics (CFD) showing that mixing of the pure oxygen stream with $CO_2$ is critical. However, as shown in the review article of Carrasco-Maldonado et al. (2016) little work has focussed on its application to cement rotary kilns which have a notable difference with boilers in that large amount of heat is provided by secondary hot gas stream coming from the clinker pre-cooler, large amount of dust are entrained in the kiln, the flame shape desired, furnace geometry and heat transfer zone are all different (see Fig. 1). A few thermodynamic studies can be found evaluating the application of oxy-fuel combustion to cement making. Hokfors et al. (2014) studied the effect of oxygen enrichment of the air, i.e. without flue gas recirculation, where the aim is not $CO_2$ capture, but improved fuel combustion. Further the same group oriented a study towards $CO_2$ capture in Hokfos et al. (2015) with 60% recirculation of flue gases to obtain a temperature in the burn zone comparable to the reference temperature and $CO_2$ concentration in the flue gases of 76% (90% water free). They concluded that the introduction of partial or full oxy-fuel combustion was possible while maintaining product quality. In Granados et al. (2015) a detailed one-dimensional model of a rotary lime kiln operating with both air combustion and oxy-fuel combustion was developed to analyse changes in decarbonation process due to energy fluxes by convection and radiation with different flue gas recirculation rates (FGR). The results indicate a temperature increase of 20% in the gas and solid phases and a higher decarbonation rate of 40% in relation to the air-combustion case. However, a compromise was found between FGR and decarbonation rate as at equal temperature the increase in $CO_2$ partial pressure promotes a reduction of the decarbonation rate. In our study, FGR is not a relevant parameter since the rotary kiln is integrated into the plant as will be described latter, therefore the flue gases are used in the calciner unit and the inlet streams come from the clinker cooler unit.

All the studies described above consider the kiln as an input/output process or at best as a 1D component with a temperature and heat transfer to the clinker profile. The assessment of flame development and streams management inside the rotary kiln is of utmost importance as flame stability, combustion properties, gas mixing and temperature distribution management impacts directly process reliability, efficiency, pollutant formation, and even feasibility. For that purpose CFD has proven to be a powerful to simulate complex geometry even at large

scale cement rotary kiln (Mastorakos et al., 1999; Wang et al., 2006). To the knowledge of the authors, only the study of Granados et al. (2014) has been reported in the peer-reviewed literature where an oxy-fuel kiln for $CO_2$ capture has been modelled. However, the rotary kiln was treated as a stand-alone unit, not connected to the rest of the plant. Granados et al. (2014) investigated the effect of FGR, between 30% and 85%, on the rotary kiln through a CFD study and found that heat transfer to the clinker could be enhanced such as specific fuel consumption could be decreased for a given clinker production rate. Since the study only considers the rotary kiln unconnected to the rest of the process, as FGR rate increases, the effects of varying mass and energy flow on the rest cement plant as a whole are ignored. In addition, flame lengths were considerably shorter and it is improbable that the requested clinker quality could be achieved with heat transfer profile so different from the air case. In the present study, the optimization procedure for the rotary kiln by CFD modelling is done in parallel with the optimization of the full cement plant. Even though not directly related to $CO_2$ capture, there are two other examples of CFD analysis of cement kiln in oxygen enriched air. Marin et al. (2001) studied a method for lancing oxygen into the kiln at a location between the load and the main burner. By looking at different injection schemes the study showed that varying the angle of the lance enables to handle various problems as reducing conditions, overheating in the burning zone or refractory wall. It was concluded that oxygen had an overall beneficial role with negligible impact on refractory temperature and the clinker. The work showed also that oxygen enrichment led to an increase in the amount of acceptable dust into the kiln. Zhou et al. (2018) covered $O_2$ enriched air up to 31% and showed that NOx formation was directly related to the increase in temperature in the flame zone, as expected from the kinetics of NO in oxygen enriched atmospheres (Samaniego et al., 1998).

Experimentally, Carrasco et al. (2019) is the only study where a specific rotary kiln burner has been tested in both air and full oxy-fuel mode at a pilot scale of 500 kW. It was observed that under oxyfuel mode parameters like total oxygen concentration and oxygen distribution in primary and secondary gas were the key variables to adjust flame formation and obtain similar results as in conventional air firing. The oxyfuel mode with 29% $O_2$ in total combustion gas resulted in similar ignition behavior and gas temperature as the reference air case. The results suggest that modern kiln burners with single jets arrangement can be suitable to switch from air firing tor oxyfuel operation without additional modifications provided that oxygen availability in primary gas is increased in the near burner area and that the swirling flows are used to improve the mixing of fuel and oxidizer to adjust flame shape and length.

To the knowledge of the authors, the present study (part of the H2020 EU project "$CO_2$ capture from cement production" - CEMCAP) is the first CFD modelling of a full scale rotary kiln in full oxy-fuel mode integrated into an entire cement plant. The study focuses on the optimization by CFD modelling of combustion in a full scale oxy-fuel retrofitted rotary kiln with oxy/air mode switching capability. The optimization criteria are flame stability, temperature, heat transfer profile to the clinker, and complete combustion. The originality of the study is that there is an additional optimization criterion based on the process optimization of the entire plant, i.e. the inlet conditions of the gas streams entering the rotary kiln are iteratively adapted according to the heat radiation profile to the material calculated by the CFD and used in the process simulation.

## 2. Methodology

### 2.1. The optimization process

The objective of the CFD simulation work is to provide the input conditions at the rotary kiln that satisfies the Best Available Technology (BAT) heat radiation to the material. The inlet conditions are a specification of the amount of gas and its composition in the different sections of the kiln and burner. On the one hand, the flame generated must provide a stable flame and a defined heat radiation profile to the clinker, on the other hand, the gas input and output streams of the rotary kiln must fulfil the overall process constraints set by the clinker cooler downstream and the calciner upstream. Therefore, the rotary kiln input conditions are then used in the process modelling (PM) work to ensure a good match with the overall cement making process. The recommended set of data reported in this study are therefore the result of an iterative optimization procedure that is described here.

To understand the procedure, it is important to be aware of the differences in the modelling tools used. The PM covers the whole cement making process illustrated in Fig. 1 from raw material to the final product including the ASU and the $CO_2$ processing unit to deliver $CO_2$ at the required purity and compressed to 130 bar. In the process the rotary kiln is only one step through which mass and energy balance is calculated, where the clinker flows and undergoes chemical and physical transformation as a result of the intense heat received during the travelling time. The rotary kiln in the PM is modelled in 1D and discretized with a few tens of elements in which a given heat radiation profile with the same resolution is imposed to the material. In contrast, the CFD simulation only simulates the rotary kiln, but solves all the fluid dynamic equations, including turbulence and chemical kinetics of the combustion process. These equations can only be solved at the microscale where mixing and combustion occurs. Therefore, the rotary kiln is simulated in 2D or 3D and discretized in millions of cells and all details of the burner geometry and boundary conditions in all directions must be included.

Both numerical tools give a material surface incident heat radiation profile along the length of the rotary kiln as an output, but because of the obvious differences in resolution and models used, these profiles can only be compared qualitatively. Besides, for one given set of inlets in the PM, there are many possibilities to distribute the primary gas at the burner. A procedure for optimizing the rotary kiln based on the two modelling tools has been developed, in which both simulations have as objective to find a solution for the material heat radiation profile in the oxy-fuel case that matches that of the reference air case. In the procedure three criteria must be fulfilled for the CFD simulations:

- Achievement of a stable oxy-fuel flame with complete combustion;
- Rotary kiln integrated heat radiation to the material is within +/- 1% of that in the reference air case;
- Flame region integrated heat radiation to the material is within +/- 10% of that in the reference air case;

Failure to achieve one of these criteria requires finding another set of input conditions at the burner and rotary kiln inlets. Upon success, the corresponding set of inlet conditions and flame characteristics are transferred for the PM. The two simulation codes are not coupled, the transfer of data is made manually. The iteration process is considered optimized when the PM results achieved are deemed satisfactory. In this article the accent is put on the combustion characteristic of an oxy-fuel rotary kiln and therefore we only present the CFD work with the results of selected simulations.

The definition of the inlet flows into the rotary kiln is not entirely free and is subject to two types of constraints, one is limited by the burner hardware design assigned by the burner supplier Thyssenkrupp, the second by a set of parameters for a cement plant defined in a framework case (Anantharaman et al., 2018). The set of constraints is summarized in Table 1 and the parameters are further described in section §2.2.1.

### 2.2. CFD setup

#### 2.2.1. The cement rotary kiln CFD model

The flow and combustion in the cement rotary kiln have been

**Table 1**
Constraints on the rotary kiln inlet conditions.

| Parameter | Constraint and comments |
|---|---|
| $O_2$ in carrier stream | 0 % - 35 % by vol. |
| Primary / secondary flow | 0.1 – 0.15 |
| Secondary $CO_2$ flow rate | 27,000 to 40,000 $Nm^3/h$ |
| Oxygen excess | 1 - 3 % $O_2$ in dry flue gases |
| Burner swirl angle | None, moveable. |
| Velocities at burner outlets | |
| Nozzles | 150 – 250 m/s |
| Secondary | 3 – 6 m/s |
| Carrier gas | 15 – 20 m/s |
| Burner hardware | Retrofit and mode switching capability |

simulated using the ANSYS Fluent 17.2 RANS code. The rotary kiln model dimensions have been setup according to a full scale 3000 t/d of cement with a total length of 60 m and inner diameter of 3.76 m, except from the clinker sintering zone (the first 20 m from the burner end of the rotary kiln) where the coating thickness increases (100 mm) reducing the diameter to 3.56 m. The CFD model is delimited at its back end by a large open entrance section where the secondary gas flows in and a burner placed at the centerline of the domain as shown in Fig. 2-a. At the opposite end corresponding to the flue gas exhaust and the entrance of the clinker, a free gas outlet is set as a boundary. The cylinder shaped kiln is bounded by a solid wall.

The burner investigated, a picture of which is shown in Fig. 2-b, is a Thyssenkrupp burner known as POLFLAME able to fit a full scale 3000 t/d rotary kiln. Coal is transported by a carrier gas stream through an annular section and the primary gas part goes through 10 adjustable swirl high velocity swirl nozzles to form the flame stabilization zone. The burner face picture shows the presence of different ports inside the high velocity nozzles region used for burner ignition and flame monitoring. These ports are not reproduced in the CFD model and are replaced by a solid wall. For simplicity, the circular nozzles, which are very small compared to the overall size of the kiln, are modelled as trapezoids having the same area to which a velocity profile with a given swirl is imposed.

Because of the general symmetry of the kiln and the burner, the computational time was greatly reduced by only simulating a $1/10^{th}$ of the entire section with periodic boundary conditions set on each sides of the simulated domain. However, it makes not possible the inclusion of both the refractory wall and the part covered by clinker material as boundaries conditions of the rotary kiln. Therefore, in these simulations the boundary conditions are set as if clinker material was covering the entire cylinder in order to capture the correct heat transfer properties between the flame and the material. This assumption is not expected to have a large impact on radiation properties since the emissivity and *Cp* of refractory walls and those of the clinker are close. The material boundary temperature in the rotary kiln was specified as a profile along the rotary kiln through a User Defined Function (UDF). The polynomial function was fit to the material top surface temperature profile (Anantharaman et al., 2018):

- For $x > 48.5$: 1116 K
- For $48.5 > x > 21.3$: $-416.10^{-6}\,x^5 + 76442.10^{-6}\,x^4 - 5452.1.10^{-3}\,x^3 + 188.21\,x^2 - 3156.5\,x + 22184$ K
- For $21.3 > x > 5.7$: $-11.9\,x + 1802$ K
- For $x < 5.7$: 1734 K

The objective of the study being to define the correct combustion properties, the clinker flow and chemistry was not modelled therefore it was not necessary to include rotation of the kiln in the simulations. To get a Cartesian grid, the centre of the combustion chamber (5 cm diameter) was cut off. This is equivalent to having a fictive 5-cm rod in the centre of the combustion chamber. The wall shear stresses on this surface was set to zero. All inlets were set up as mass-flow inlets, while the outlet was set as a pressure outlet. After controlling that the further modification of the grid had no impact on the major variables as temperature, radiation profile and main species in terms of maximum and outlet values, the resulting mesh consisted of 1,648,500 cells. In addition to standard convergence criteria in ANSYS Fluent, stable temperature and mass flow at the kiln outlet was used. Simulations of the different cases used the previous case and results as starting point. Achieving a new stable solution took an average of 15 000 iterations over approximately 24 h on 12 cpus in parallel on a linux machine with

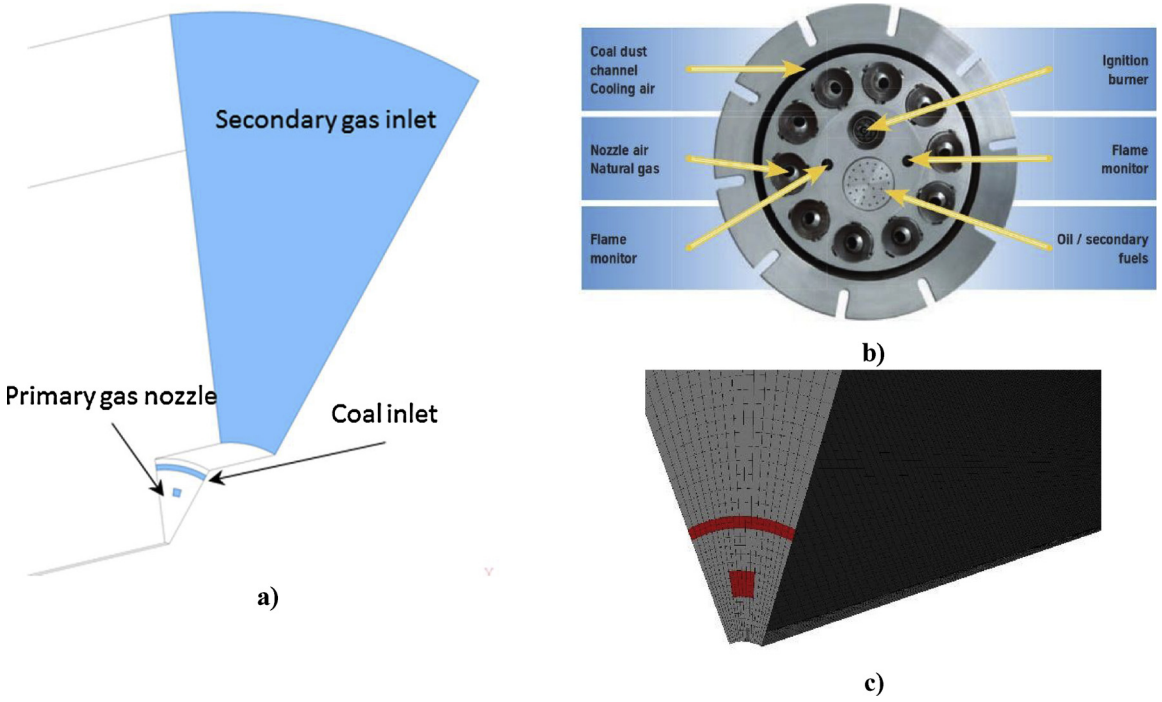


**Fig. 2.** a: CFD model of the rotary kiln back end; b: the Thyssenkrupp POLFLAME burner; c: detail at the burner face.

Intel Xeon E5-2643 v3 @ 3.40 GHz. To achieve a solution from no start field took about 48 h.

The range of allowable burner parameters was based on the current burner design where priority is given to keeping the flow velocities at each outlet within a certain range (cf. Table 1) as these are detrimental to the desired operation of the burner (impulse and swirl effect). The flow inputs parameters were refined during the optimization procedure described in section §2.1 within the range given in Table 1.

Before initiating the simulation of the full-scale rotary kiln, a preliminary study was performed meant as a selection and validation of the CFD setup. As there are no available measurement detailed enough from full scale kilns, the validation study was done against experiments at a lower, yet relevant scale of 500 kW with the same design, but downscaled burner. It is important to validate at an appreciable scale in order to scale up with confidence, however the shortcoming is that measurement accuracy and control of inputs become more challenging. In addition, the grid was necessarily different form the full-scale case. Nevertheless, the validation work allowed to test the procedure for grid preparation, convergence and select the different models used. The profiles of species and temperature showed some quantitative mismatch with the experiments, attributed to the general tendency of higher combustion rate, the uncertainty and resolution of the measured dataset, and most importantly the extra air flow rates due to leakages and flame detector cooling in the experiments. The incident heat radiation profiles seen in Fig. 3 for the oxy-fuel and air cases, show the different zones and the transition from the near field (steeply increasing) to the region where the radiation flattens and are relatively well reproduced (given the above limitations) although the peak heat radiation is more pronounced in the CFD. In the experiments, the measured incident heat radiation falls steeply due to higher heat loss. It is generally observed that CFD simulations (particularly RANS) fail to reproduce the degree of intermittency occurring in large scale flames which can be controlled by real non-uniformities of the flows and boundary conditions. Time averaged measurements over periods greater than the largest scales of turbulence (as in the case of gas sampling methods and thermocouple measurements) inevitably result in a spatial averaging bias and smooth zones with high gradient. The flame shape is generally well reproduced by the CFD and the model set up was considered as validated for simulating the full-scale flames with the degree of accuracy required to support the process simulation.

### 2.2.2. The fuel and turbulent combustion model

Preliminary CFD work at a smaller scale was done to select a set of models. These simulations were validated against boiler pilot testing with a down scaled version of the same burner performed at the University of Stuttgart at a thermal power input of 500 kW in air and oxy-fuel modes (Carrasco et al., 2019). The models selected and used in the full scale simulations are listed in Table 2 and in Table 3 for the fuel properties. The gas phase is modelled using RANS, the particle phase

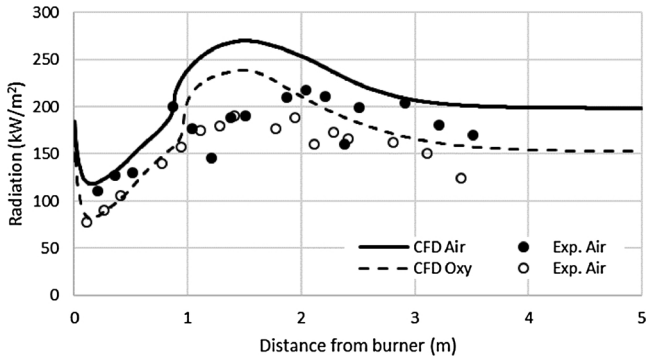


**Fig. 3.** Comparison radiation profiles on a 500 kW petcoke fired boiler. Experimental data from H2020 CEMCAP Project.

with a Lagrangian approach, and their interaction with a spherical drag law. The coal particle distribution is handled through a Rossin-Rammler size distribution method. The combustion model considers coal particles to devolatilize first, then volatiles and char burn. In addition to the default one-step reaction for volatiles available in the CFD code, six additional reactions have been included in order to have a better accuracy on the combustion behaviour in oxy-fuel mode, particularly for the CO kinetics which is known to be limiting. The seven chemical reactions are:

$$\text{Volatiles} + 2.01\ O_2 \text{ - > } 1.2\ CO_2 + 2.2\ H_2O + 0.02\ N_2 + 0.02\ SO_2 \quad (1)$$

$$H_2 + 0.5\ O_2 \text{ - > } H_2O \quad (2)$$

$$CO + 0.5\ O_2 \text{ - > } CO_2 \quad (3)$$

$$CO + H_2O \text{ - > } CO_2 + H_2 \quad (4)$$

$$C(s) + 0.5\ O_2 \text{ - > } CO \quad (5)$$

$$C(s) + CO_2 \text{ - > } 2CO \quad (6)$$

$$C(s) + H_2O \text{ - > } H_2 + CO \quad (7)$$

Eqs. (1)–(4) are gas phase combustion reactions, while Eqs. (5)–(7) are heterogeneous reactions to model char burnout. The 4 gas phase reactions are modelled through the Finite rate/Eddy Dissipation model. The reactions leading to $SO_2$ and $N_2$ are only present in Eq. (1) and are produced as soon as the solid particle has devolatized and starts to burn. Even though the reaction rate parameters could be adapted to reflect the high concentration of $CO_2$, a conventional setup has been selected as it has negligible effect on large scale parameters according to the review of Chen et al. (2012). Shaddix and Molina (2009) also showed that the effect of $CO_2$ on kinetic properties like ignition delay time was mostly due to its higher heat capacity.

Oxidizer streams are composed of air or oxygen from the ASU and $CO_2$ coming from the condenser. The oxidizer is injected at the burner gas inlets through the high velocity nozzles, as the fuel carrier and at the back end of the rotary kiln as secondary gas coming from the clinker cooler. Marin et al. (2001) showed that dust insufflation into the kiln had an impact such as reduced temperature profile, resulting in a less stable combustion process. Therefore, to simulate the effect of clinker dust heavily present in real rotary kilns, inert particles (with emissivity of 0.9) were introduced together with the secondary gas stream. The presence of high partial pressure of tri-atomic gases requires that the conventional WSGGM parameters used for air combustion be adapted to account correctly for gas radiation in oxy-fuel mode. There is considerable literature showing that effect and several sets of parameters have been proposed. However, in this study the conventional air WSGGM has been used primarily because in the case of rotary kiln for cement application, there are large amounts of solid particles from the coal fuel itself and from the dust carried in through the secondary streams and present throughout the whole kiln length. The studies of Andersson et al. (2008) and Johansson et al. (2013) have showed experimentally and numerically by using the Mie theory and gas radiation modelled using the statistical-narrow-band model that in the case of coal combustion, solid particle radiation is largely dominating over gas radiation, let alone in the case with additional dust amount as in this study. Similar results were obtained in the study of Bäckström et al. (2015) in a down-scaled pilot of an iron ore kiln furnace. Solid particle radiation is here taken into account, therefore for the purpose of this study the simplification of using the conventional WSGGM was considered acceptable.

A total of ca. 15 cases were run with the purpose of improving the simulation quality and then the iteration against PM as described in the methodology (cf. §2.1). The rotary kiln inlet flow input parameters used in the reference air case and in selected two oxy-fuel cases of the optimization process are shown in Table 4.

**Table 2**
Models used in the CFD.

| | |
|---|---|
| Turbulence | k-omega SST |
| Chemistry | Species transport, Finite rate/Eddy-Dissipation, 7 reactions, ideal gas |
| Radiation | Discrete Ordinates and Weighted Sum of Gray Gases Model (WSGGM) |
| Solver | Pressure based Coupled solver with Pseudo-transient model enabled |
| Rotary kiln material boundary | Temperature profile for BAT air reference case Anantharaman et al. (2018) |

**Table 3**
Coal properties.

| Property (Units) | Value | Coal ultimate analysis (water and ash free) | Value |
|---|---|---|---|
| HCV (J/kg) | 27,150 | | |
| Volatiles (% by mass) | 27 | C (% by mass) | 83.15 |
| Fixed C (% by mass) | 56 | H (% by mass) | 4.82 |
| Ash (% by mass) | 16.5 | O (% by mass) | 10.85 |
| Moisture (% by mass) | 0.5 | N (% by mass) | 0.58 |
| Coal size (μm) | 100 – 400 | S (% by mass) | 0.60 |
| **Combustion model parameters** | | | |
| Particle emissivity (-) | 1 | | |
| Vaporization temperature for volatiles (K) | 600 | | |
| Binary diffusivity ($m^2/s$) | $4.10^{-5}$ | | |
| Particle scattering factor (-) | 0.9 | | |
| Swelling coefficient (-) | 1.4 | | |
| Reaction of heat absorbed by solid (%) | 30 | | |
| Constant rate devolatilization model (1/s) | 12 | | |

**Table 4**
CFD simulations inlet properties of selected cases.

| Cases: | | AIR | OXY-1 | OXY-2 |
|---|---|---|---|---|
| Oxidizer | | $O_2/N_2$ | $O_2/CO_2$ | $O_2/CO_2$ |
| **Primary gas** | | | | |
| Volume flow rate | $Nm^3/h$ | 5,100 | 4,500 | 4,500 |
| Temperature | K | 323 | 323 | 323 |
| $O_2$ | % | 21 | 60 | 60 |
| Velocity | m/s | 250 | 221 | 221 |
| Swirl degree | angle | 20° | 30° | 30° |
| **Carrier gas** | | | | |
| Volume flow rate | $Nm^3/h$ | 4,040 | 1,600 | 1,050 |
| Temperature | K | 323 | 323 | 323 |
| $O_2$ | % | 21 | 30 | 18 |
| Velocity | m/s | 38.3 | 15.2 | 10.0 |
| Coal mass flow rate | kg/s | 1.469 | 1.469 | 1.469 |
| **Secondary gas** | | | | |
| Volume flow rate | $Nm^3/h$ | 29,090 | 36,000 | 28,126 |
| Temperature | K | 1073 | 1073 | 1273 |
| $O_2$ | % | 21.0 | 18.0 | 20.8 |
| Velocity | m/s | 3.7 | 4.6 | 4.3 |
| ***Flue gas composition*** | | | | |
| $O_2$ | *% dry* | *1.1* | *4.6* | *3.0* |
| $N_2$ | *% dry* | *80.8* | *0.0* | *0.1* |
| $CO_2$ | *% dry* | *18.1* | *95.3* | *96.9* |
| $H_2O$ | *% wet* | *6.0* | *5.5* | *6.9* |
| ***Results*** | | | | |
| *Flame length (1400C)* | *m* | *17.0* | *16.0* | *16.8* |
| *Max incident heat location* | *m* | *6.8* | *7.3* | *7.7* |
| *Gas exit temperature* | *K* | *1065* | *1111* | *1079* |
| *Max gas temp. location* | *m* | *10.0* | *8.3* | *8.6* |

## 3. Results and discussion

Both OXY-1 and OXY-2 cases fulfilled the criteria defined in the methodology (cf. §2.1) regarding flame stability and heat distribution in the rotary kiln and were therefore considered to be optimized from the CFD's perspective, however OXY-2 was the preferred setup from a PM point of view. The combustion is complete as the mass fraction of major species at the outlet plane of the CFD simulation domain are equal to that from the mass balance with full conversion within less than 0.5%. Table 4 also gathers the outlet values in the flue gas. Most of the results presented in the remainder are those of the optimized OXY-2 and air reference cases.

### 3.1. Flame dimension and radiation profile

Two flame size characteristics are necessary as input to the PM: the flame length and shape. There are several ways for measuring flame length experimentally, it can be done visually through observable intensity of luminosity, by measuring a species or temperature profile along the flame centreline (Ditaranto et al., 2001; Sautet et al., 2001). In this study, we define the flame length at the point in the streamwise direction where the decreasing mean temperature profile crosses 1400 °C. This is also the definition that was used in the ECRA CCS project (European Cement Research Academy, 2012) and it is near the inflexion point in the streamwise temperature decay. Results for the reference and the last two oxy-fuel cases are 17.0 m, 16.0 m, and 16.8 m for the reference air, OXY-1, and OXY-2 cases respectively. The flame shapes obtained are qualified as triangular for the flames investigated as can be seen in the example given in Fig. 4. The triangular aspect is a result of the expanding flow generated by the strong swirl.

Surface incident heat radiation at the material is a critical characteristic of the rotary kiln flame as the clinker quality strongly depends on it. Fig. 5 shows the surface incident heat radiation profiles for the reference air case and the two optimized oxy-fuel cases. From around 20 m to the rotary kiln end (i.e. material inlet), there is little variation between the cases because this region is mainly composed of mixed hot gases homogenous in composition and temperature. The differences are more marked in the first 20 m region corresponding to the flame where the distribution of temperature and species are controlled by the burner inlet conditions in terms of inlet velocity, composition, and degree of swirl. The rotary kiln integrated incident heat radiation to the material are deviating by -0.8% and 2.1% from that of the reference case for the optimized oxy-fuel cases OXY-1 and OXY-2 respectively. When integrated over the near flame region the corresponding deviations are -7.9% and 2.0%. These deviations are within the criteria of 1% and 10% for the OXY-1, but higher for the overall flame for OXY-2 (2.1% against 1%). This deviation was however accepted for further processing.

Table 4 shows the differences in the primary gas stream between the reference air and oxy-fuel cases, showing that the total available gas in the primary stream is one third lower in the oxy-fuel case. It must be noted that the primary gas needs be cooled, therefore it is important to minimize the flow rate of this stream as it has an energy efficiency cost. This requirement has to be combined to the constraint on the burner which must have high swirling velocity jets in order to shape the flame and provide good stabilization at the nose of the burner. As a result, most of the flow reduction in the primary stream has been applied to

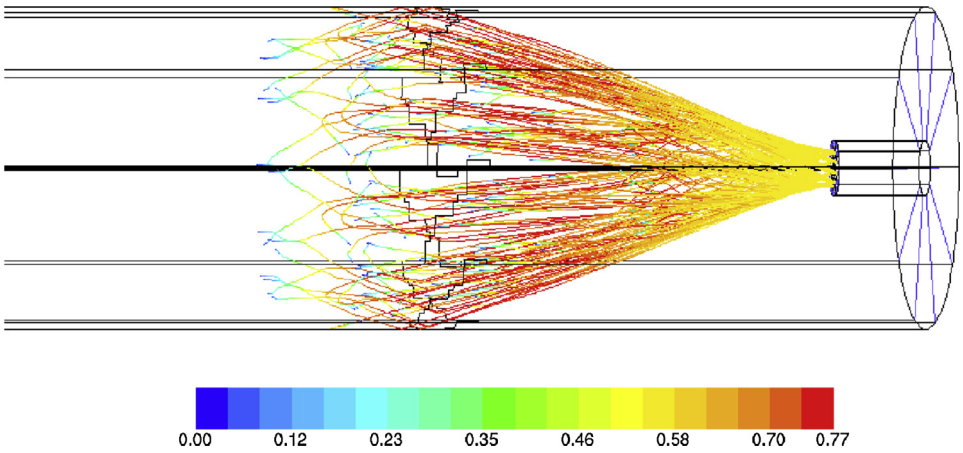


**Fig. 4.** Char particles trajectories and mass fraction in case OXY-2 showing the "triangular" flame shape in the near burner region.

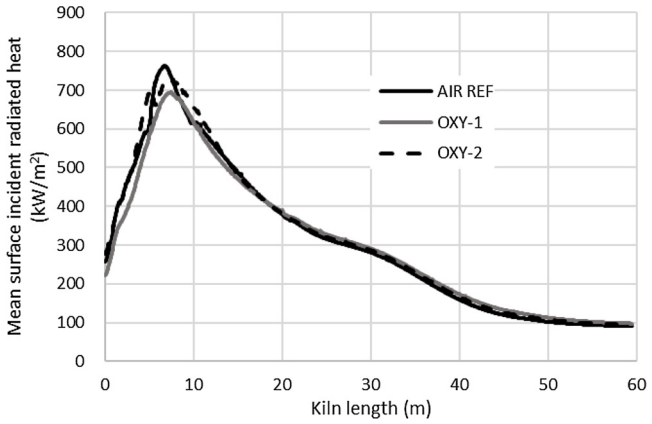


**Fig. 5.** Surface incident heat radiation profile at the rotary kiln boundary for the three cases.

the carrier gas flow. The degree of swirl has been increased to compensate for the lower velocity achieved. Another noticeable difference is the oxygen concentration at the nozzle which is as high as 60% in the oxy-fuel cases, although the oxygen concentration in the primary gas is at best 52% if primary and coal carrier gas streams were perfectly mixed.

The results show that the same burner can be used in both air and oxy-fuel modes, making it flexible for mode shifting purposes and a good retrofit hardware, but it is at the expense of significant variation in inlet conditions. It is seen in Fig. 5 that in the reference air case, the clinker receives a higher peak radiation intensity than in the oxy-fuel case, being the location where most of deviation in the integrated heat radiation is. Attempts to further reduced the deviation would have forced one or several of the following measures:

- Further enriching the primary stream in oxygen.
- Further increasing the swirl degree.
- Further decreasing the carrier flow velocity (in order to increase the velocity in the primary stream nozzle).

Such modifications would result in what is considered as a too large deviation from the burner originally intended conditions and were therefore not pursued since the defined acceptance criteria of these OXY-cases were already achieved. Burner hardware modifications would also be a solution, but it had to be overlooked here because of the planned retrofit application for this study. Finally, another parameter that could be varied to improve the fit is the primary gas temperature, but it is however not free for modification according to the constraint definition of Table 1.

### 3.2. Near burner flame characteristics

The previous section showed the results of the optimization procedure from a process point of view with clearly defined criteria that the oxy-fuel case should fulfil. These criteria are macroscopic effect of the flame on the material, however the oxy-fuel flame obtained has strong structural difference as compared to the reference case. In this section we highlight the differences in the near burner region, that is the region where the flame is stabilized in a complex turbulent fluid dynamic pattern.

#### 3.2.1. Temperature field

The temperature maps of Fig. 6 show the structure of the flame with a slightly more expanding flame front in the oxy-fuel case and a stabilization of the flame at approximately the same distance from the burner. The flame even seems to be attached to the outer wall in the OXY-2 case. It seems improbable from a physical assessment that there may be a stabilisation point downstream the flame itself, but the wall can have an indirect stabilizing effect through creation of a recirculation zone, as often seen in swirl burner with low expansion ratio. Be aware that the contour plot of Fig. 6 is a cross section, looking at OXY-2 in the 3D illustration of Fig. 7 shows that the structure at the point away from the burner of seemingly stabilization at the wall (i.e. at the second X-Y plane from the burner exit) has a more complex structure and that the flame is mostly concentrated well within the kiln wall. Concerning the cold region around the centreline in the near field, it is seen from the burner configuration illustrated in Fig. 2-b that the coal particles are injected in the annular section on the outside of the high-speed jets creating the swirling motion, it is therefore not so surprising that the particles are ejected radially and ignite in the hot (1273 K) secondary oxidizer stream. Note that the air case has a lower swirl angle with a consequently lower degree of expansion. A RANS-turbulence model artefact over-expanding the flame zone should not be excluded too, but it is difficult to say which effect is dominant.

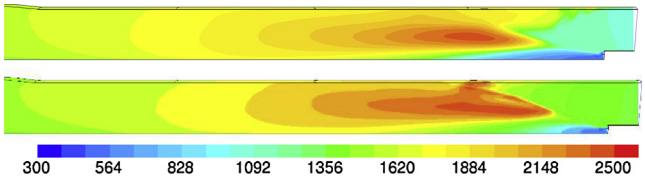


**Fig. 6.** Contour maps of temperature (K) in the mid-plane crossing the nozzle centreline. Air reference (top) and OXY-2 (bottom) cases. Total kiln length is 60 meters.

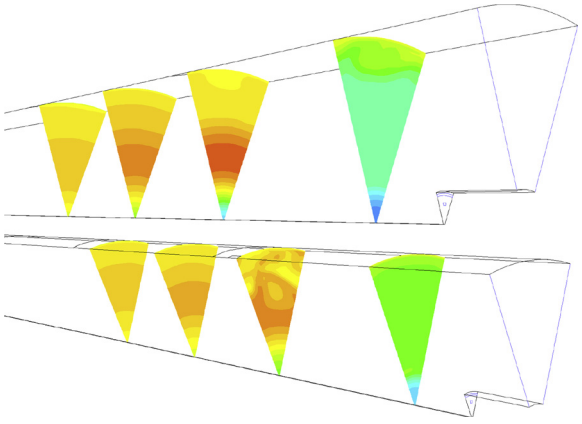

**Fig. 7.** Temperature (K) cross section maps at 2 m, 5 m, 7.5 m, and 10 m from rotary kiln burner end. Air reference (top) and OXY-2 (bottom) cases (same colour scale as in Fig. 6).

The most striking difference is in the peak temperature reaching a higher value in the air case (2360 K against ca. 2239 K) although the primary gas composition in the oxy-fuel case is as high as 60% in the oxy-fuel case (cf. Table 4). Even though the secondary stream in OXY-2 has a somewhat higher temperature than in the air case, this result appears as a paradox knowing the strong dependence of the adiabatic flame temperature on oxygen concentration in the oxidizer. For the sake of comparison, methane burning in these two oxidizer compositions would have a difference in adiabatic flame temperature of nearly 475 K in favour of the oxy-fuel case. The observed peak temperature difference is truly responsible for the higher peak heat radiation felt by the material also observed in Fig. 5. To understand this phenomenon it is necessary to look deeper in the flame structure and analyze how combustion evolves from the injection of cold coal particles to fully burned.

The maximum temperatures seem high, probably overestimated due the relative simplicity of the models having a tendency to burn too rapidly. To the knowledge of the authors, no local flame front temperature data in real kiln is available. A study in a 500 kW boiler reported in Carrasco et al. (2019) revealed measured temperature up to 1620 K, in boiler conditions and at a much lower scale. Strangely, they measured the same maximum temperature at 20%, 40% and 60% oxygen in the oxidizer. In measurements with intrusive probes, there is a spatial averaging bias due to the highly turbulent large flames which makes the peak temperature unmeasurable even though they may exist on very small scale.

Fig. 7 is a three-dimensional representation of the flame temperature field highlighting the non-homogeneity of the flame in the radial and tangential directions up to at least 5 m downstream the burner, where the presence of the swirling high velocity jet can still be seen. One observes in Fig. 6 that the air flame reaches homogeneity sooner because the gas streams, primary, secondary and carrier gas, have all the same composition. As such, the longitudinal cross-section at the mid-plan is misleading.

### 3.2.2. Species

Oxygen concentration maps are given in Fig. 8 showing clearly the more complex oxidizer distribution at the beginning of the rotary kiln in the oxy-fuel case, due to the strong difference in inlet compositions of the three gaseous mixtures (primary, carrier, and secondary streams). Corresponding maps of CO concentrations are shown in Fig. 9. There the differences are also very much marked due to the particular chemistry of $CO_2$. Glarborg and Bentzen (2008) have highlighted the impact on CO formation of high $CO_2$ concentration on the gas phase chemistry and Saanum and Ditaranto (2017) have experienced how mixing and residence time in various temperature regions can generate large concentrations in the exhaust gases. The situation is even more critical in coal combustion as in addition to the aforementioned homogeneous chemistry, three heterogeneous reactions of char which are modelled in these simulations (Eqs. (5)–(7) in §2.2.2) are strong producers of CO. Particularly so when $CO_2$ is present at large partial pressures in the so-called Boudouard reaction (Eq. (6)) which net production reaction rate is two orders of magnitude larger in the oxy-fuel case. This dependency was also clearly observed experimentally in Carrasco et al. (2019) who performed measurements in the 500 kW down-scaled version of the burner at varying oxygen concentration in the primary gas where peak CO concentrations were more than doubled compared to the air case.

Near the kiln boundary, a high CO concentration spot can be observed and can be explained by the flow dynamic pattern of the coal particles shown in Fig. 4. It is seen that part of the char formed during devolatization has not gasified completely before they hit the rotary kiln boundary. In addition, the CO concentration cross section maps of Fig. 10 show that at that distance from the burner, the flow and species distributions are still under the strong effect of the swirling motion and not homogenously mixed in the radial direction. The high CO spot at the solid surface is therefore due to a quenching of the homogeneous CO reduction reactions.

### 3.3. Temperature paradox

As highlighted in section §3.2.1, the higher peak temperature attained in the air case constitutes a paradox given the much higher oxygen concentration in the primary oxidizer composition and corresponding higher flame adiabatic temperature. The oxygen concentration fields shown in Fig. 8 give a possible explanation for that phenomenon. Indeed, the oxygen concentration in the range of 60% are not to be seen anywhere in the domain, but at the primary gas outlet plane.

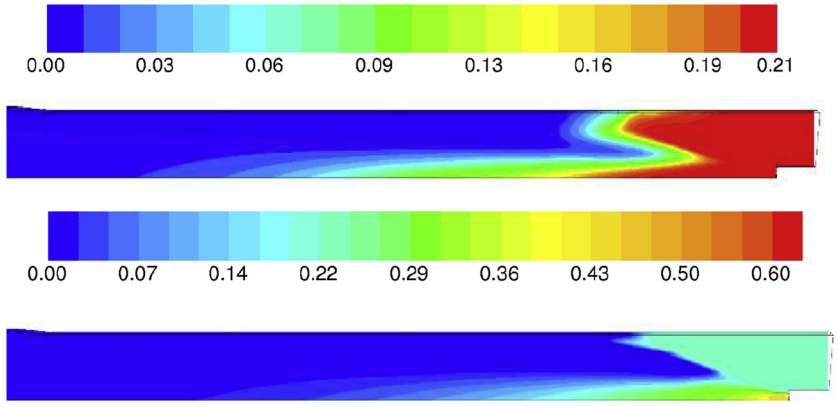


**Fig. 8.** Contour maps of $O_2$ volume fraction in the plane crossing the nozzle centerline. Air reference (top) and OXY-2 (bottom) cases.

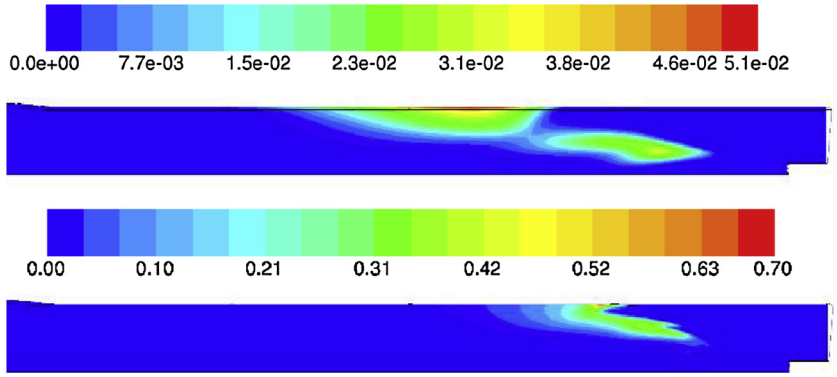


**Fig. 9.** Contour maps of CO volume fraction in the mid-plane crossing the nozzle centerline. Air reference (top) and OXY-2 (bottom) cases.

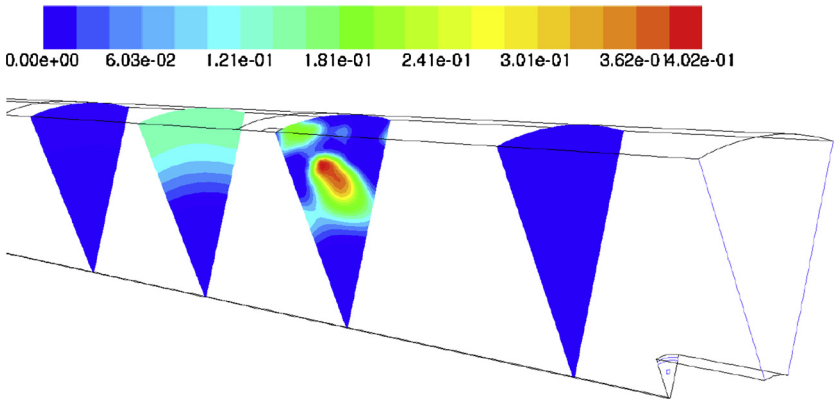


**Fig. 10.** CO (volume fraction) cross section maps at 2 m, 5 m, 7.5 m, and 10 m from rotary kiln gas end. OXY-2 case.

The primary flow becomes very soon diluted, first by the carrier gas surrounding the coal particles, and then mostly by the large amount of secondary gas only containing 20.8% $O_2$ in $CO_2$. The temperature map shows that the combustion reactions are mostly stabilized at around 2.4 ms away from the burner and at approximately 1.4 m off the centreline, giving enough time for the primary flow to be diluted to an $O_2$ concentration of ca. 25–29 %. At these concentrations, it is indeed expected that the flame temperature in $CO_2$ would be lower than in air, explaining thus the apparent paradox.

### 3.4. Flame stabilization and heat radiation profile

The location of the combustion stabilization zone is controlled by the time needed for the coal to reach devolatilization temperature as seen in the plot of char mass fraction of Fig. 4. On the other hand, it has been shown above that because the secondary stream has a much lower $O_2$ concentration, the further away from the burner, the lower the $O_2$ concentration in the overall oxidizer stream (due to dilution of primary by secondary gas stream). As a consequence, increasing the primary gas temperature, would result in shortening the devolatilization zone, hence stabilize the flame in a region of higher $O_2$ concentration, which in turn would generate a higher peak temperature and gas heat radiation rate to the material. This point highlights another lever to control the heat radiation profile and the importance of a correct model selection.

## 4. Conclusions

The study performed and presented herein has been customized as to answer the objective of the optimization procedure in parallel with process modelling work which simulated the entire cement making process, for finding an optimized set of inlet conditions at the rotary kiln. A fair balance was found and considered acceptable between the level of detailing and accuracy of the models, and the numerical expense in terms of CPU time and efforts to achieve converging cases. Following the agreed optimization procedure, several CFD simulations for a reference air case and various oxy-fuel cases. The optimization process led to the set of input parameters (streams inlet flow rates, temperatures, compositions, swirl angle) generating a stable flame providing an optimal radiation heat profile to the clinker similar to that in the reference case. In order to provide such a heat radiation profile, the oxy-fuel flame length and temperature distribution in the rotary kiln are different from that in the reference air case due to the different fluid properties. The suitable oxygen concentration in the primary gas and secondary gas streams found were 52.1% and 20.8% respectively. According to the simulations, the POLFLAME burner is a burner that can be used for retrofit applications and allows mode switching, where only the swirl angle of the high velocity nozzles needs be adjusted when shifting from air to oxy-fuel mode, something that is possible with the burner hardware. It is recommended that further studies consider unwanted air entries in the rotary kiln and the secondary gas stream (through the pre-cooler), such as their effect on NOx and gas properties to the calciner, and further to the flue gas cleaning unit, can be better assessed.

## Acknowledgements

This publication has received funding from the European Union's Horizon 2020 research and innovation programme under grant agreement No 641185. Authors are particularly grateful to the project team members from University of Stuttgart (F. Carrasco-Maldonado, J. Maier), Thyssenkrupp (E. Willms), and VDZ (A. Jamali, J. Ruppert) for discussions and advise during the work presented in this publication.

## References


European Cement Research Academy, 2009. ECRA CCS Project: Report About Phase II.

Adamczyk, W.P., et al., 2017. CFD modeling and thermodynamic analysis of a concept of a MILD-OXY combustion large scale pulverized coal boiler. Energy 140, 1305–1315.

Anantharaman, R., et al., 2018. CEMCAP Framework for Comparative Techno-economic Analysis of CO2 Capture From Cement Plants - D3.2. Zenodo.

Andersson, K., et al., 2008. Radiation intensity of lignite-fired oxy-fuel flames. Exp. Therm. Fluid Sci. 33 (1), 67–76.

Bäckström, D., et al., 2015. On the use of alternative fuels in rotary kiln burners — an experimental and modelling study of the effect on the radiative heat transfer conditions. Fuel Process. Technol. 138, 210–220.

Buhre, B.J.P., et al., 2005. Oxy-fuel combustion technology for coal-fired power generation. Prog. Energy Combust. Sci. 31 (4), 283–307.

Carrasco, F., et al., 2019. Experimental investigations of oxyfuel burner for cement production application. Fuel 236, 608–614.

Carrasco-Maldonado, F., et al., 2016. Oxy-fuel combustion technology for cement production - State of the art research and technology development. Int. J. Greenh. Gas Control. 45, 189–199.

Chen, L., Yong, S.Z., Ghoniem, A.F., 2012. Oxy-fuel combustion of pulverized coal: characterization, fundamentals, stabilization and CFD modeling. Prog. Energy Combust. Sci. 38 (2), 156–214.

Deja, J., Uliasz-Bochenczyk, A., Mokrzycki, E., 2010. CO2 emissions from Polish cement industry. Int. J. Greenh. Gas Control. 4 (4), 583–588.

Ditaranto, M., Sautet, J.C., Samaniego, J.M., 2001. Structural aspects of coaxial oxy-fuel flames. Exp. Fluids 30 (3), 253–261.

European Cement Research Academy, 2012. ECRA C.C.S. Project – Report on Phase III.

Gerbelova, H., van der Spek, M., Schakel, W., 2017. Feasibility assessment of CO2 capture retrofitted to an existing cement plant: post-combustion vs. oxy-fuel combustion technology. In: Dixon, T., Laloui, L., Twinning, S. (Eds.), 13th International Conference on Greenhouse Gas Control Technologies, Ghgt-13, pp. 6141–6149.

Glarborg, P., Bentzen, L.L.B., 2008. Chemical effects of a high CO2 concentration in oxy-fuel combustion of methane. Energy Fuels 22 (1), 291–296.

Granados, D.A., et al., 2014. Effect of flue gas recirculation during oxy-fuel combustion in a rotary cement kiln. Energy 64, 615–625.

Granados, D.A., Chejne, F., Mejia, J.M., 2015. Oxy-fuel combustion as an alternative for increasing lime production in rotary kilns. Appl. Energy 158, 107–117.

Hills, T., et al., 2016. Carbon capture in the cement industry: technologies, progress, and retrofitting. Environ. Sci. Technol. 50 (1), 368–377.

Hokfors, B., Eriksson, M., Viggh, E., 2014. Modelling the cement process and cement clinker quality. Adv. Cem. Res. 26 (6), 311–318.

Hokfos, B., Viggh, E., Eriksson, M., 2015. Simulation of oxy-fuel combustion in cement clinker manufacturing. Adv. Cem. Res. 27 (1), 42–49.

IEAGHG(TCP), 2013. Deployment of CCS in the Cement Industry.

IEAGHG(TCP), 2018. Technology Roadmap - Low-carbon Transition in the Cement Industry.

IPCC, 2006. IPCC Guidelines for National Greenhouse Gas Inventories 2006.IPCC Guidelines for National Greenhouse Gas Inventories 2006.

Johansson, R., et al., 2013. Influence of particle and gas radiation in oxy-fuel combustion. Int. J. Heat Mass Transf. 65, 143–152.

Leeson, D., et al., 2017. A Techno-economic analysis and systematic review of carbon capture and storage (CCS) applied to the iron and steel, cement, oil refining and pulp and paper industries, as well as other high purity sources. Int. J. Greenh. Gas Control. 61, 71–84.

Marin, O., et al., 2001. Simulating the impact of oxygen enrichment in a cement rotary kiln using advanced computational methods. Combust. Sci. Technol. 164, 193-+..

Mastorakos, E., et al., 1999. CFD predictions for cement kilns including flame modelling, heat transfer and clinker chemistry. Appl. Math. Model. 23 (1), 55–76.

Saanum, I., Ditaranto, M., 2017. Experimental study of oxy-fuel combustion under gas turbine conditions. Energy Fuels 31 (4), 4445–4451.

Samaniego, J.M., et al., 1998. Mechanism of nitric oxide formation in oxygen-natural gas combustion. Twenty-Seventh Symposium (International) on Combustion Vols. 1 and 2, 1385–1392.

Sautet, J.C., et al., 2001. Length of natural gas-oxygen non-premixed flames. Combust. Sci. Technol. 166, 131–150.

Schneider, M., et al., 2011. Sustainable cement production-present and future. Cem. Concr. Res. 41 (7), 642–650.

Shaddix, C.R., Molina, A., 2009. Particle imaging of ignition and devolatilization of pulverized coal during oxy-fuel combustion. Proc. Combust. Inst. 32 (2), 2091–2098.

Toftegaard, M.B., et al., 2010. Oxy-fuel combustion of solid fuels. Prog. Energy Combust. Sci. 36 (5), 581–625.

Wang, S.J., et al., 2006. Modeling of pulverized coal combustion in cement rotary kiln. Energy Fuels 20 (6), 2350–2356.

Zheng, L.Y., Hills, T.P., Fennell, P., 2016. Phase evolution, characterisation, and performance of cement prepared in an oxy-fuel atmosphere. Faraday Discuss. 192, 113–124.

Zhou, Y., et al., 2018. Simulating the process of oxy-fuel combustion in the sintering zone of a rotary kiln to predict temperature, burnout, flame parameters and the yield of nitrogen oxides. Chem. Technol. Fuels Oils 54 (5), 650–660.